A New Framework for Multi-Hop ABS-Assisted 5G-Networks With Users' Mobility Prediction

Elhadja Chaalal , *Student Member, IEEE*, Sidi-Mohammed Senouci , *Member, IEEE*, and Laurent Reynaud, *Senior Member, IEEE*

Abstract—Unmanned Aerial Vehicles (UAVs) have gained momentum as one of the potential solutions in 5 G networks. Indeed, using UAVs as Aerial Base Stations (ABS) to assist the traditional cellular infrastructure and/or extend its coverage represents a high-potential flexible and cost-effective approach to provide on-demand communications in these new generations of networks. Yet, their effective deployment brings out many challenges, including their optimal 3D placement, coverage optimization, backhaul constraints, etc. Hence, we tackle these challenges by proposing a new framework for 3D positioning of an ABS swarm in order to extend the coverage of ground base stations (GBS). Unlike existing work that ignore ABS's limited backhaul capacity and how it restraints the number of users that can be served, we consider a multi-hop backhaul scheme that allows ABSs to remain connected to the core network through the GBSs directly, or other deployed ABSs. Under this setup, we aim to maximize the number of served UEs, by optimizing the ABS's placement, jointly with their association with UEs and backhauling base stations. Besides, our framework, named ASF for Adaptive Social Spider Optimization based framework, uses machine learning techniques to predict the users' mobility and enable ABSs to adjust their position according to their spatial distribution. Simulations show that ASF framework significantly improves the cellular network's coverage and provides access to 92% of mobile users, as compared to other benchmark schemes that only serve 79% and 58% of users.

Index Terms—UAV, aerial base stations, adaptive framework, multi-hop backhauling, social spider optimisation, machine learning, mobility prediction.

I. INTRODUCTION

THE rapid spread of highly capable wireless devices such as smartphones, tablets and IoT-style gadgets, that are accessing mobile networks worldwide has led to an unprecedented surge in mobile data traffic. Indeed, the latest analytic forecasts indicate that the total number of global mobile devices will grow to 13.1 billion by 2023, whilst there were 8.8 devices

in 2018 [1]. As a consequence, the existing wireless cellular networks' coverage and capacity have been widely strained. Thus, next-generation communication systems (5 G and beyond) must develop intelligent heterogeneous architectures and tools capable of handling the explosion in mobile traffic volumes, extending the wireless cellular coverage and providing guaranteed quality of service (QoS) to mobile users.

Under such circumstances, UAV-assisted wireless networks have emerged as a complement for heterogeneous 5 G environments and a promising solution to overcome this challenge. In fact, UAVs are being deployed as aerial base stations (ABS) to assist the cellular network in providing a good quality of experience or seamless coverage to ground users [2], as they have the ability to provide reliable, cost-effective and on-demand wireless communication to ground users, especially when the ground communication facility is inaccessible. Compared to terrestrial base stations, using UAVs as aerial base stations has the following advantages:

- First, as its altitude increases, the ABS experiences more line-of-sight (LOS) connections toward ground base stations and users. ABSs can effectively complement existing cellular systems by providing additional capacity and enhance coverage and rate performances, [3].
- Then, owing to their high mobility and agility, ABSs can avoid obstacles and adjust their position in order to increase the probability of LoS links and thus provide a quick, flexible and on-demand wireless communication,
- Moreover, ABSs are less expensive than traditional communication infrastructures making them more convenient to achieve rapid service recovery when ground infrastructures are damaged in natural disasters such as hurricanes, floods, and earthquakes [4].

Given such unique features, using UAVs as ABSs can boost the performance of existing ground cellular network, and be an integral part of future next generation networks [5]. However, leveraging the potential of ABSs requires overcoming numerous practical challenges [6]. For instance, the 3D placement of ABSs [2], air-to-ground channel modeling [7], trajectory optimization [8], etc. In particular, the optimal 3D placement of ABS is a challenging issue that has attracted significant attention from the research community. The majority of prior works focused on the optimization of their deployment locations for communication performance improvement [2, 9-11]. In [9] and [10], the authors consider a set of ABSs hovering at the same altitude, and study the placement problem of ABS in

the horizontal plane. 3D positioning of ABSs can be obtained easily by introducing the altitude dimension as in [2], [11] where numerical and heuristic solutions were proposed. Yet, the challenging backhaul connectivity of ABSs to the core network is overlooked by current articles, where authors ignore the backhaul link as in [12], or consider a predefined fixed limited backhaul rate and bandwidth as in [13]. Unlike a ground BS, that has a strong reliable wired/wireless backhaul connection, an ABS in the sky can't have a wired connection but only a wireless backhauling link can be employed for connecting it to the core network. Wireless backhaul links are highly susceptible to interference originating from a wide variety of sources, such as adverse weather conditions and other small / macro cells, which restraints the number of users that can be served, and is affected by the UAV's position regarding to the BS that provides the backhaul connection to the core network. Moreover, the mobility of ground users is neglected by existing work. The motivations of this work are concluded as follows:

- Providing ABSs with satisfactory, reliable backhaul connections to the core network is a challenging task to be addressed, which was ignored by existing works that only focused on optimizing the air-to-ground access link between ABSs and ground users,
- A mobility of ABSs that considers the mobility of users on the ground was not studied in most existing contributions, which only consider the placement of several ABSs, while users on the ground are assumed to be static,
- Three-dimensional dynamic movement of ABSs has not been investigated in most current contributions, which mainly consider ABSs hovering at a same fixed altitude. The 3D placement and position adjustment of ABSs needs to be considered to reap the full potential of ABSs.

To fill such a research gap, we study a general multi-hop ABS-assisted 5G-wireless communication system, where a swarm of ABSs is employed to serve a group of mobile users on the ground in a given area. Although a single ABS has demonstrated its advantages in performance enhancement for wireless networks [14]-[15], it has a limited capability in general and may not guarantee availability during the entire mission. Our previous work in [16] studies the problem of placing a swarm of ABSs to extend the GBS's coverage while maintaining a direct backhaul link between ABSs and GBSs. We aim to extend this work and consider that ABSs are connected via wireless multi-hop backhaul scheme with the core network where the ABSs can get wireless backhaul connections from other ABSs in order to serve more ground users and cover larger areas. Moreover, the case of dynamic wireless networks where the users freely move and significantly change positions overtime wasn't addressed either. To this end, we propose a new adaptive placement algorithm to maximize the number of served users without continuously monitoring their locations. The continuous monitoring may cause a large amount of overhead, and the ABSs decision coordination may not be accurate enough due to users' mobility. Therefore, mobility prediction would be a better choice to estimate the users' location, as every person's movement has a certain degree of regularity that makes it predictable. A study in [17] shows that human mobility patterns have a high degree of spatial and temporal regularity and that it is centered around a small number of locations such as home, workplace, favorite shop, etc. Under this setup, our objective is to optimize the multiple ABS's 3D placement, in order to extend the ground network's coverage, subject to such rate-constrained wireless backhaul connections. To the best of our knowledge, this problem has not been studied yet. To fill such a research gap, we propose a multi-hop adaptive social spider optimization-based framework for the 3D aerial base station placement, for coverage extension. The contributions of this paper can be summarized as follows:

- We present and model a realistic constrained multi-hop scenario where UAVs are used as ABSs along traditional GBSs to extend their coverage. Our model considers the different interference among ABSs, GBSs, and user equipment (UEs) and uses reliable 3GPP models to simulate signal propagation and compute SINR (Signal to Noise and Interference Ratio) values. Besides, it considers the limited wireless backhaul that an ABS can get from the GBSs. Therefore, the ABSs can be used as relays to provide backhaul connection to other ABSs,
- We propose an adaptive framework for the multi-hop ABSs placement in order to maximize the number of covered UEs. It is based on the Social Spider Optimization meta-heuristic that determines the ABSs position while maintaining a direct backhaul link with the GBS,
- We study the user's mobility in wireless networks and use efficient machine learning models to predict the users' distribution. The results of mobility prediction are used by the multi-hop framework to enhance its performance and allow it to adjust the ABSs positions accordingly,
- We provide in depth simulations that were conducted considering various scenarios and evaluated to validate the proposed framework.

The remainder of this paper is structured as follows: Section II provides an overview of the literature related to the challenges of using UAVs as ABS. Section III introduces the system model and the problem formulation of the multi-hop ABS placement for coverage extension in 5 G wireless networks. In Section IV we describe the efficient multi-hop adaptive SSO-based framework (ASF) for 3D placement of ABSs that relies on a single-hop placement metaheuristic. Section V studies the users' mobility and presents the proposed machine learning models to predict their mobility in order to adjust the ABS's placement. Section VI presents the numerical results to demonstrate the performance of the proposed framework. Finally, we conclude the paper in Section VII.

II. RELATED WORK

Despite the promising opportunities for deploying ABSs, a non negligible number of technical challenges arises and has to be addressed to effectively leverage their potential in the next generation of wireless networks. Main challenges could be scattered around: optimal ABS deployment, channel modeling, trajectory optimization, and network planning. We describe these challenges in the following.

A. Optimal ABS Placement

The adjustable location of ABSs is a major asset to design rapid and flexible on-demand wireless links to ground users. However, the three dimensional deployment of ABS is quite challenging as ABSs can be deployed in a continuous 3D space. Besides, ABSs locations directly affect the channel quality [14] and the performance of the provided wireless network, consequently. Therefore, optimal deployment of ABSs for coverage extension, capacity maximization, public safety or IoT applications has attracted significant interest. Two main scenarios can be distinguished:

1) Single ABS Placement: In [14] and [15], the 3D placement of a single ABS, providing wireless network to a set of users is considered. The objective is to maximize the number of covered users. The problem in [14] is formulated as a quadratically-constrained mixed integer non-linear optimization problem, and a numerical solution is proposed to solve it. While in [15], it is modeled as a circle placement and smallest enclosing circle problem under the constraint of minimizing transmit power. In [18], the optimal positioning of an ABS acting as a relay between a GBS and a fixed position user in a dense urban area is investigated. The authors used the line-of-sight propagation characteristics with the objective of maximizing the network's capacity.

The authors in [19] study the effectiveness of integrating ABS into cellular networks as an alternative to the deployment of ultra-dense small cells. They consider a scenario where a single ABS is deployed to assist the ground base station and serves a group of moving users. Authors [20] investigated the optimal altitude of a single ABS, yielding in a maximum coverage radius. They show that finding the optimal ABS altitude must consider the impact of both distance and LoS probability simultaneously. Work in [21] considered a wireless network where an ABS is deployed as a relay between a transmitter and a receiver. The objective is to determine the optimal location of the ABS that maximizes the average rate.

2) Multiple ABSs Placement: Simultaneously deploying multiple UAVs is more challenging due to the impact of inter-cell interference. In [9] and [10], the authors consider a set of ABSs hovering at the same altitude, and the placement problem of ABS is studied in the horizontal plane. In [9], they propose an optimization model to efficiently place the ABSs, in order to maximize the number of covered users and minimize the communication cost between ABSs. [10] consider a fleet of ABSs covering a set of mobile sensors and reporting information to a ground. The optimal placement of UAVs was solved with an optimization model that first reduces the number of variables and solves the resulted problem using column generation. 3D positioning of ABSs can be obtained by introducing the altitude dimension as in [2] where numerical and heuristic solutions were proposed. In [2], the authors propose a framework that uses a swarm of ABSs to assist a ground cellular network of uniformly distributed users. It places the ABSs according to a network planning approach based on stochastic geometry. Work in [12] extended the work in [20] and considered the problem of covering a ground area using two ABSs, and investigated the impact of the altitude and the distance between ABSs on coverage. Numerical expressions for optimal altitude and distance allowing maximum coverage are proposed in both interference-free and full interference scenarios. In [11], both drone base stations and drone users are considered. A truncated octahedron shapes-based method is proposed for the 3D placement of ABSs and the optimal cell association is then defined using optimal transport theory to minimize drone users' latency. In [22], multiple ABSs are used as relays to enhance the connectivity of a ground wireless network. In particular, they studied the optimal deployment of ABSs to guarantee sensors' message delivery to destinations. Similarly, authors in [23] studied the deployment of a set of ABSs as relays to provide wireless network service for ground sensors. They investigated the trade-off between connectivity among the ABSs and the maximization of the served area.

B. Channel Modeling

The air-to-ground channel possesses different characteristics from ground-to-ground channels [24] as it highly depends on the ABS altitude and the propagation environment. As a consequence, designing a generic channel model for ABS-to-ground (A2G) communication is challenging and requires extensive simulations and measurements in different environments. Much recent research investigated the A2G channel modeling. In particular, a series of studies is proposed in [7] for the characterization of path loss, small-scale fading, and delay spread models for A2G channels in different environments. The measurements were carried out at seven different ground sites, ranging from over-water sites to hilly and mountainous sites, to suburban and quasi-urban sites. In [25], a comprehensive loss model and a Ricean fading model for high altitude platforms are proposed, based on modeling and simulations. [26] proposed a statistical propagation model for communications between high altitude platforms and ground users in an urban environment. LoS and NLoS links are considered and the associated probabilities of occurrence are derived. In [27], a theoretical model is proposed to determine the LoS probability for A2G links in an urban environment. They formulate the problem as a function of building heights and size, street distribution, and elevation angle. The model seems to agree with ray-tracing simulations. The A2G path loss model proposed in [28] is one of the most wildly adopted models to describe the communication link between low altitude platforms and ground users. Depending on the ABS and user locations and the type of the propagation environment, the link can be LoS or NLoS. A probabilistic model is then considered to derive the associated probabilities of occurrence. The probability of occurrence depends on the environment, the height and density of buildings, and elevation angle between ABS and ground users. A comprehensive survey of recent channel measurements and modeling efforts to characterize the A2G channel for UAVs can be found in [29].

C. Path Planning

Exploiting the ABS high mobility allows cellular networks to unlock the full potential of ABS-assisted networks. However, ABS trajectory design and optimization are challenging as they require investigating an infinite number of possible

ABS locations [30]. Trajectory optimization in ABS-assisted wireless networks is considered more challenging. Indeed, it has to simultaneously process both mobility and QoS metrics constraints. For this reason, it has been the subject of several studies that consider the relationship between ABS trajectory and wireless network performance. In [8], the authors consider a wireless communication system where a set of ABSs is serving a group of ground users. The authors optimized the ABSs trajectory and maximized the average minimum throughput of ground users. The problem is formulated as a mixed-integer non-convex optimization problem. In a similar scenario, a path planning algorithm for ABSs with multiple antennas is proposed in [31] to maximize the overall throughput in uplink communications. The work in [32] proposed a novel cyclical multiple access scheme, where a single ABS flies above ground users and communicates with them in a periodic (cyclical) time-division manner. Significant throughput gains have been achieved over static ABS scenarios. Moreover, the optimal trajectory of an ABS acting as a relay in a wireless network is studied in [33], where the sum-rate is jointly maximized along with the transmit power. In [34], trajectory optimization for ABSs in a search and localization scenario is studied. In this work, path planning is analyzed by maximizing the likelihood of target detection. Finally, a generic mobility model for a fleet of inter-connected ABSs that collaborate to explore a geographic area is proposed in [35].

D. Network Planning

Network planning entails many issues such as backhaul management, user-cell association, frequency allocation, and interference mitigation, etc. It becomes more challenging in the context of ABS-assisted wireless networks due to ABS mobility, limited wireless backhaul connectivity, and LoS interference. The user-ABS association in ABS-based cellular networks is addressed in [36], [37] and [2]. The work of [36], [37] aims to find the minimum required number of ABS and their association with ground users to maximize the network coverage and capacity, respectively. While in [2], the objective is to provide the user's required rate using minimum ABS transmit power. Authors in [38] investigate the optimal cell partitioning between ABSs and ground base stations. Optimal transport theory tools are used to solve the association problem. Unlike ground base stations, which have a strong reliable wired/wireless connection with the core network, untethered flying ABSs require a wireless backhaul link to connect with the core network. Wireless backhaul is highly susceptible to interference originating from a wide variety of sources, such as adverse weather conditions, other small cells, and macro-cells. Considering the high probability of LoS communication between ABSs and ground base station, millimeter-wave and free-space optical communications (FSO) are promising solutions for ABS wireless backhauling [39]. Authors in [13] consider the 3D placement of ABSs to maximize coverage and the average rate of users link under a predefined fixed limited backhaul rate and bandwidth constraints. Moreover, an analytical expression for the probability of backhaul
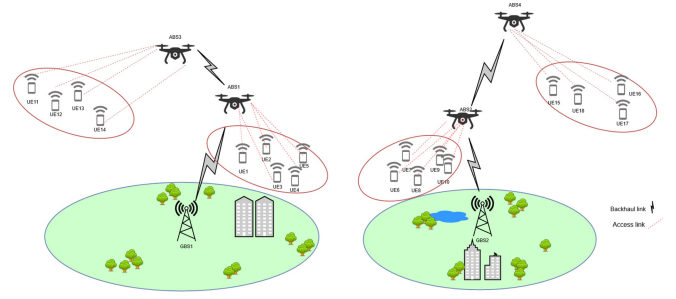

Fig. 1. System model.

connectivity for ABSs that can use either an LTE or a millimeter-wave backhaul is derived in [40]. WiFi and satellite links are also used for ABS wireless backhaul [41]. WiFi-based links are less expensive and have a lower latency compared to satellite links that have a wider coverage range.

Table I outlines for each challenge related to ABS deployment and cited above, the key references, the covered issues and the main used methods. As can be seen, 3D-ABS positioning was highly studied under network performance constraints. However, existing works don't investigate the problem along with other challenges, such as trajectory optimization or wireless backhauling. Therefore, we decided to tackle the challenging problem of positioning a set of ABSs with a limited wireless backhaul that strongly depends on the ABS position, regarding to its serving base station (BS), whether GBS or ABS. Moreover, we consider a high dynamic wireless network where users freely move and change positions over time. Consequently, ABSs adjust their position and adapt it to the users' spatial distribution.

III. SYSTEM MODEL AND PROBLEM FORMULATION

In this section, we first present the considered wireless communication system, define channel models and finally formulate the problem of positioning a set of ABSs in order to extend coverage and serve a maximum number of users.

A. System Description

We consider a wireless communication system, where $K \geq 1$ GBSs are deployed to cover and provide access in a certain region. A limited group of $M \geq 1$ UAVs is made available and acts as dynamic ABSs to extend the GBS coverage and provide access to the subset of $N \geq 1$ moving uncovered single-antenna UEs. Each ABS must remain connected to a GBS by a sufficiently high-speed backhaul, that guarantees information exchange and traffic offload with negligible delays. Therefore, a subset of ABS is deployed as relay nodes, to provide backhaul link to the core network for other ABS as illustrated in Fig 1.

For ease of implementation, we consider a wireless short-backhaul, point-to-point Sub-6 GHz spectrum connection in order to connect the ABSs to the core network. Short-haul solutions are used in the access and aggregation backhaul segments over short distances ranging between several hundred feet to 10 miles, which is suitable for our use case. The GBS, UE, and ABS sets are denoted as **K**, **N** and **M**, respectively, where $| \mathbf{K} |= K,$

TABLE I
ABS-ASSISTED WIRELESS NETWORKS: CHALLENGES, REFERENCES, COVERED ISSUES AND USED TOOLS

Challenges	Key references	Covered issues	Tools and techniques
3D placement	[15] [16], [17], [18] [20] [8] [9] [10] [2], [11] [19], [21] [22]	- Deployment in the presence of terrestrial networks - Effect of ABS altitude on the network performance - Joint 3D placement optimization and QoS maximization - Joint 3D placement and user-ABS association	- Centralized optimization theory - Optimal transport theory - Stochastic geometry
Channel modelling	[23] [6] [24], [25] [26], [27] [28].	- Air-to-ground channel modeling - Air-to-ground path loss modeling - LoS and NLoS probabilities - Small scale fading modeling	- Extensive measurement - Ray-tracing - Probabilistic models
Trajectory optimization	[29], [7], [30] [31] [32] [33]	- Energy-efficient trajectory optimization - Joint trajectory and QoS optimization	- Centralized optimization theory - Machine learning
Network planning	[36] [2]. [35], [37] [38]. [12] [39]. [40]	- Joint trajectory optimization and user-ABS association. - Joint trajectory and transmit power optimization. - ABS backhauling	- Centralized optimization theory - Optimal transport theory - Facility location theory

$| \mathbf{N} | = N, | \mathbf{M} | = M$. The GBSs fixed positions are defined as $V = \{v_1, v_2, v_3, \ldots v_k\}$, while the coordinates of mobile ABSs and UEs at time slot t are given by $U = \{u_1^{(t)}, u_2^{(t)}, u_3^{(t)}, \ldots u_m^{(t)}\}$ and $Y = \{y_1^{(t)}, y_2^{(t)}, y_3^{(t)}, \ldots y_n^{(t)}\}$, respectively.

We consider a downlink scenario in which each ABS in the set $\mathbf{M}$, schedules transmission over contiguous time-frequency slots, which are referred to as Resource Blocks (RB), each consisting of a block of orthogonal frequency-division multiplexing sub-carriers and symbols. Frequency Division Multiplexing Access (FDMA) assigns individual frequency bands to RBs; each user has its dedicated channel for communications, which allows that they do not interfere with one another. The transmitting power of ABS $m \in \mathbf{M}$ on each RB is assumed to be constant.

Our objective is to find the optimal strategy for the placement of the ABSs, that takes into account high dynamic user mobility. Therefore, for efficiency, each user's location must be predicted. At each time slot, we use the user's position data history during the last T time slots to predict the user's position at the following T' time slots. The input vector is given as a time-series $Y = \{y_i^{(1)}, y_i^{(2)}, \ldots, y_i^{(T)}\}$ of length T, where each point $y_i^{(j)} \in R^2$ is a 2-D vector of the user i coordinates at the time instance t_j. The output result is also a time-series $Y' = \{y_i'^{(T+1)}, y_i'^{(T+2)}, \ldots, y_i'^{(T+T')}\}$ of length T' where each point $y_i'^{(T+j)} \in R^2$ represents a 2-D vector of the user's i predicted location at the next instance t_{T+j}.

B. Transmission Model

We denote the channel power gain between a transmitter i and a receiver j at time slot t by: $G_{ij}^{(t)} = L_{ij}^{(t)} . F_{ij}^{(t)}$ Where $L_{ij}^{(t)}$ is the large scale slow fading component, that captures the effects of path-loss and shadowing, and $F_{ij}^{(t)}$ represents the small-scale fast-fading component that simulates the effects of rapid amplitude fluctuations when the receiver travels a distance of a few wavelengths. We adopt a set of reliable models for the characterization of the wireless channels between GBSs, ABSs, and ground users. These models were proposed, tested, and approved by the 3rd generation partnership project (3GPP), or in trusted scientific papers. Accordingly, for communication between:
- An ABS and a UE, we use the channel model in [28],

- An ABS and a GBS, we use the channel model from the 3GPP technical specifications [42],
- A GBS and a UE, we use the channel model from the 3GPP technical specifications [43],
- Two ABSs, we use the channel model proposed in [44]

The total power of the signal that a UE n receives from an ABS m at a time slot t is given by the sum of the useful transmitted signal, the interference with other ground or/and aerial transmitters, and the thermal noise. Thus, the instantaneous $SINR$ from ABS m to user n on an RB is calculated as: $SINR_{mn}^{(t)} = \frac{P_m^{(t)} G_{mn}^{(t)}}{\sum_{i \neq m} P_i^{(t)} G_{in}^{(t)} + \sum_{j \in K} P_j^{(t)} G_{jn}^{(t)} + \delta^2}$ where $P_m^{(t)}$ and $P_i^{(t)}$ are transmission power of ABSs m and i, respectively. $P_j^{(t)}$ is the transmission power of the GBS j and δ^2 denotes the thermal noise spectral power.

The reachable throughput of a UE n served by ABS m can be directly calculated from its achievable $SINR$, by using Shannon expression [45]: $R_{m,n} = B_0 \cdot \log_2(1 + SINR_{m,n})$ where B_0 denotes the bandwidth over which the RB is realized. Note that the n-th UE may be served by an ABS m if it experiences SINR equal to or higher than the minimum required SINR: $SINR_{mn}^{(t)} \geq SINR_{min}$

In the same way, the instantaneous received $SINR$ of the backhaul link of an ABS l from a GBS k at time slot t is given by: $SINR_{kl}^{(t)} = \frac{P_k^{(t)} G_{kl}^{(t)}}{\sum_{i \neq l} P_i^{(t)} G_{il}^{(t)} + \sum_{j \neq k} P_j^{(t)} G_{jl}^{(t)} + \delta^2}$ where $P_k^{(t)}$ and $P_j^{(t)}$ represent the transmission power of GBSs k and j, respectively. $P_i^{(t)}$ is the transmission power of the ABS i.

Hence, the capacity of the backhaul link between an ABS l and a GBS k can be written as: $R_{kl}^{(t)} = W \log_2(1 + SINR_{kl}^{(t)})$ where W denotes the backhaul link's bandwidth.

Moreover, the instantaneous received $SINR$ of the backhaul link of an ABS l from another relay ABS m at time slot t is given by: $SINR_{ml}^{(t)} = \frac{P_m^{(t)} G_{ml}^{(t)}}{\sum_{i \neq l} P_i^{(t)} G_{il}^{(t)} + \sum_{j \in k} P_j G_{jl}^{(t)} + \delta^2}$ where $P_m^{(t)}$ and $P_i^{(t)}$ are transmission power of ABSs m and i, respectively. $P_j^{(t)}$ is the transmission power of the GBS j.

Hence, the capacity of the backhaul link that an ABS l receives from another ABS m, over the air-to-air channel can be expressed as: $R_{ml}^{(t)} = W \log_2(1 + SINR_{ml}^{(t)})$ where W denotes the backhaul link's bandwidth.

C. Energy Consumption Model

The total energy consumption of an ABS involves two elements:

- Communication energy: consists of the required energy for signal transmission and radiation, signal processing, circuitry, etc.
- Propulsion energy: consists of the required energy for hovering the ABS and supporting its mobility, if needed.

Usually, the communication energy is ignored, as it is much smaller than the propulsion energy (few watts [46] versus hundreds of watts [47]). Moreover, the required propulsion energy of a fixed-wing UAV under normal operations is a function of its trajectory $U(t)$. Therefore, we adopt the energy consumption model in [48], as it does not imply any constraints on the type of trajectory and expresses the UAV's consumed energy along its trajectory $u(t)$ as a function of its velocity $v(t)$ and acceleration $a(t)$ vectors ((1)):

$$
E(u(t)) = \int_0^t \left[c_1 \|v(t)\|^3 + \frac{c_2}{\|v(t)\|} \left(1 \right. \right.
$$
$$
\left. \left. + \frac{\|a(t)\|^2 - \frac{(a^T(t)v(t))^2}{\|v(t)\|^2}}{g^2} \right) \right] dt + \frac{1}{2} m(\|v(T)\|^2 - \|v(0)\|^2)
\tag{1}
$$

where c_1 and c_2 are two parameters related to the UAV weight, wing area, air density, etc., g is the gravitational acceleration with nominal value $9.8 m/s^2$, m is the mass of the UAV including all its payload.

Assuming that between every two time slots t and $t+1$ the ABS flies directly from $u(t)$ to $u(t+1)$ following a straight line, the instantaneous ABS velocity becomes constant $v(t) = \frac{\|u(t+1)-u(t)\|}{(t+1)-t}$ and the acceleration vector equals zero $a(t) = 0$. Accordingly and based on (1), the required propulsion energy for an ABS to travel from $u(t)$ to $u(t+1)$ follows a linear model and can be expressed as follows:

$$
E(u(t), u(t+1)) = \int_t^{t+1} \left[c_1 \|v(t)\|^3 + \frac{c_2}{\|v(t)\|} \right] dt
\tag{2}
$$

Moreover, the ABS's required propulsion energy to travel from its initial location $u(0)$ to any other location $u(t)$ is calculated as the sum of the required propulsion energy to travel between each two adjacent positions:

$$
E(u(0), u(t)) = \sum_{i=0}^{i=t-1} E(u(i), u(i+1))
\tag{3}
$$

The optimization of the ABS energy consumption is out of the scope of this paper. Instead, we considered a replacement strategy, where the ABS is replaced by another fully charged ABS, whenever it reaches a predefined threshold σ. This threshold depends on the capacity of the UAV's battery, its controller position, and its distance from the mission area. As in [48], we consider $c_1 = 9.62 \times 10^{-4}$ and $c_2 = 2250$

D. Problem Formulation

In this section, we formulate the problem of finding the 3D coordinates of a limited number of ABSs at each time slot t in order to extend the cellular network coverage and hence maximize the number of covered mobile UE.

We first define the instantaneous user association indicator $I_{nm}^{(t)}$ as:

$$
I_{nm}^{(t)} = \begin{cases} 1, & \text{if user } n \text{ is served by ABS } m \text{ at instant } t \\ 0, & \text{otherwise} \end{cases}
$$

Consequently, the total number of served UEs can be calculated as:

$$
S^{(t)} = \sum_{n \in N} \sum_{m \in M} I_{nm}^{(t)}
$$

Similarly, the instantaneous backhaul-association indicator $J_{lk}^{(t)}$ can be expressed as:

$$
J_{lk}^{(t)} = \begin{cases} 1, & \text{if ABS } l \text{ gets backhaul from BS } k \text{ at instant } t \\ 0, & \text{otherwise} \end{cases}
$$

k can either be an aerial or a ground base station. Due to the multi-hop architecture, each ABS-backhauling connection is subject to the so-called flow conservation constraints, i.e., the total out going flow from each ABS (to ground users through the access links or to other ABS through air-to-air backhauling links) should be no larger than the total incoming flow to that ABS (from the ground base station or from other backhauling ABS).

Accordingly, the required backhaul capacity for ABS m can be expressed as the sum of the served users' rate along with the sum of the required backhaul of the other l ABSs that are getting backhaul from m, denoted hereafter as $Z_l^{(t)}$:

$$
Z_m^{(t)} = \sum_{n \in N} I_{nm}^{(t)} R_{mn}^{(t)} + \sum_{l \in M} J_{lm}^{(t)} Z_l^{(t)}
\tag{4}
$$

Given this system model, the goal is to find an effective optimal 3D positioning of ABSs as well as the joint association of UEs with their serving ABSs and the ABSs with the ground/aerial base stations providing backhaul link J that maximizes the number of covered UEs and meets the backhaul requirements of each ABS. We formulate the problem as:

$$
\max_{U^{(t)}, I^{(t)}, J^{(t)}} \sum_{n \in N} \sum_{m \in M} I_{nm}^{(t)}
\tag{5}
$$

subject to:

$$
Z_m^{(t)} \le \sum_{k \in K \cup M} J_{mk}^{(t)} R_{km}^{(t)} \quad \forall m \in M
\tag{6a}
$$

$$
\sum_{m \in M} I_{nm}^{(t)} \le 1 \quad \forall n \in N
\tag{6b}
$$

$$
\sum_{k \in K \cup M} J_{mk}^{(t)} \le 1 \quad \forall m \in M
\tag{6c}
$$

$$
\frac{u_m^{t+1} - u_m^t}{(t+1) - t} \le V_{max} \quad \forall m \in M
\tag{6d}
$$

$$E(u_m(0), u_m(t)) \leq \sigma \quad \forall m \in M \qquad (6e)$$

where $U^{(t)} = (u_1^{(t)}, u_2^{(t)} \ldots u_m^{(t)})$ denotes the 3D coordinates of each ABS $i \in M$ at time slot t: $u_i^{(t)} = (x_i^{(t)}, y_i^{(t)}, h_i^{(t)})$. (6a) models the flow conservation constraint and ensures that the access and backhaul provided by an ABS don't exceed its backhaul capacity, (6b) ensures that a UE can't be served by more than one ABS, while (6c) expresses that an ABS can't get a backhaul from more than one BS. (6d) limits the UAVs' moving distance conforming to their allowed speed. Finally, (6e) ensures that each UAV's energy consumption does not exceed the predefined threshold σ.

This problem strongly depends on the positions of the users and requires permanent adjustments of the ABSs location, the ABSs/users association as well as the ABSs backhaul association according to users' mobility. Note that the positions of ground users change over time as the distribution of ground users varies in real-time. Yet, humans' mobility has a high degree of spatial and temporal regularity that makes it predictable. Therefore, it is necessary to predict the users' distribution and mobility over the target area where the ABSs will be deployed accordingly. In the next section, we propose a solution to optimally deploy the ABSs and solve the problem (5), then we introduce the machine-learning algorithms that we used to predict the users' mobility.

IV. OPTIMIZATION OF ABSs PLACEMENT

As explained in Section III, the location of users is collected once every time slot τ. Therefore, we facilitate the ABSs trajectory optimization by dividing the flight duration into T time slots with equal length. The length of each time slot is τ. At the beginning of each time slot, the users' distribution for the next T' time slots is predicted and the position of ABSs is calculated accordingly(We detail the prediction algorithms in the next section). Technically, once the users' locations for the next T' time slots are predicted, the ABSs can solve the previously defined optimization problem and determine their optimal 3D deployment as well as the joint association with UEs and serving base stations corresponding to each time interval. We assume that the ABSs positions don't change during each time slot. In the following, we presnte the architecture of the proposed multi-hop adaptive SSO-based framework for the definition of the 3D coordinates of multiple ABSs to extend the GBSs coverage.

A. Adaptive SSO-Based Framework for ABS's Placement

We propose an Adaptive algorithm to jointly optimize the position of ABSs and their association with both UEs and backhauling BSs. As a first step, a single-hop ABS placement scenario is considered. In other words, the ABSs can only have a direct backhaul link with the ground base stations. This initial step is formulated in the next section and solved using a meta-heuristic called Social Spider Optimization. Once the ABSs are optimally placed, some pf them cannot get a sufficient backhaul connection from the GBSs, and remain unused, or serving a very small number of users.

Algorithm 1: Adaptive SSO-based Framework for Multi-Hop ABSs Placement.

1: Inputs: The sets of GBSs K, ABSs M and UEs N
2: Output: position of ABSs
3: **repeat**
4:   Run SSO on the sets K, M and N (Algorithm 3)
5:   $N' \leftarrow unserved\_users$
6:   $K' \leftarrow \emptyset$
7:   **for** each ABS i **do**
8:     **if** $|users\_served\_by(i)| \leq limit$ **then**
9:       $M' \leftarrow M \cup i$
10:       $N' \leftarrow N' \cup users\_served\_by(i)$
11:     **else**
12:       $K' \leftarrow K' \cup i$
13:   $K \leftarrow K'$; $M \leftarrow M'$; $N \leftarrow N'$
14: **until** $K = \emptyset$ or $M = \emptyset$ or $N = \emptyset$

So, at a next step, already deployed ABSs with sufficient resources will act as GBSs and become anchor BSs that provide backhaul links to other unused ABSs to extend the coverage and realize a multi-hop backhaul scheme. This can be formulated as a single-hop placement problem if we consider the already deployed ABSs as GBSs that provide direct backhaul communication to the unused ABSs. The problem is then solved using the same SSO heuristic. The proposed adaptive SSO-based framework (ASF) alternates between two steps: the single hop positioning and the adaptation and post-optimization steps until the terminating condition are satisfied:
1) Single-hop ABSs positioning: we only consider the direct backhaul link between ABS and GBS. The ABSs positions that maximize the total number of served users are determined using the optimization heuristic, SSO.
2) Adaptation and post-optimization: based on the results of the previous step, we formulate the problem of positioning the remaining ABS as a single-hop placement problem; we identify the remaining unserved set of users N'. We then identify the set of ABSs M' that are not deployed or serving a very small number of users. The already deployed ABSs K' are considered as GBSs and will provide a direct wireless backhaul link to the M' ABSs in order to serve the remaining N' users. The objective of this step is to prepare the next execution of the previously mentioned heuristic.

The number of iterations corresponds to the number of hops and is defined by the terminating condition. This latter is satisfied when no ABS is underused or if all backhaul connections are overloaded. Algorithm 1 shows the pseudo-code of this adaptive framework.

B. SSO Algorithm for Single-Hop 3D ABSs Placement

As explained above, we consider a scenario where ABSs only get direct backhaul link from a GBS or previously deployed ABS considered as GBSs. By doing so, the expression of required backhaul capacity in (4) of each ABS m changes. By substituting it in 6a, and considering the positioning of ABSs for a single

time slot τ, the problem of single-hop 3D ABS placement can be expressed as:

$$\max_{U^{(\tau)}, J^{(\tau)}} \sum_{n \in N} \sum_{m \in M} I_{nm}^{(\tau)} \quad (7)$$

subject to:

$$\sum_{n \in N} I_{nm}^{(\tau)} R_{nm}^{(\tau)} \leq \sum_{k \in K} J_{mk}^{(\tau)} R_{mk}^{(\tau)} \quad \forall m \in M \quad (8a)$$

$$\sum_{m \in M} I_{nm}^{(\tau)} \leq 1 \quad \forall n \in N \quad (8b)$$

$$\sum_{k \in K} J_{mk}^{(\tau)} \leq 1 \quad \forall m \in M \quad (8c)$$

where constraint (8a) denotes that an ABS can't provide more access than its backhaul capacity, constraints (8b) and (8c) ensure that a UE can't be served by more than one ABS and an ABS can't get backhaul from more than one GBS. Due to the binary variables I, J, and continuous variables U, the aforementioned ABSs positioning, and joint user and backhaul association problem are considered as mixed-integer nonlinear programming (MINLP) problems. MINLP problems face the difficulties of both of their sub-classes, i.e., the combinatorial nature of mixed-integer programming (MIP) and the difficulty in solving nonlinear programming (NLP). Since both MIP and NLP are NP-hard, our ABSs placement problem is NP-hard and can't be solved in a polynomial time. Such problems are often addressed by using approximation methods and heuristics. Therefore, we propose to adapt the metaheuristic method, Social Spider Optimisation (SSO) [49], to this problem. This choice is justified by the fact that SSO has demonstrated its efficiency and scalability on many NP-hard optimization problems [50].

SSO is a recent swarm metaheuristic that is based on an iterative process. We generate and classify an initial population of solutions. Each solution is represented by a male or female search agent (spider). At each iteration and in order to explore efficiently the search space, the set of female and male spiders attempt to reach the optimal position, they move according to their respective cooperative operators. The information about the encountered solutions is then exchanged by emitting vibrations over the communal web. Nearby male and female members mate, thereby forming new offspring solutions. The population is then updated and the worst members are replaced by the resulting broods. The process finishes when a fixed number of iterations, without improvement of the actual population, is reached. The best solution is then returned. The main steps of our adapted SSO are:

1) Population initialisation,
2) Spider's evaluation,
3) Information exchange,
4) Moving spiders,
5) Mating operator.

We describe these steps in the following.

1) Population Initialisation: To model the highly female-biased characteristic of the social spiders' population, the number of female members N_f is computed as follows: $N_f = floor[(0.9 - rand \cdot 0.25) \cdot pop_{size}]$.

Algorithm 2: UEs Association Algorithm.

1: Input: The positions of GBSs, ABSs, and UEs
2: Output: L_i list of UEs served by each ABS i
3: Compute the SINR between each ABS and GBS.
4: Associate each ABS i to the GBS with the highest SINR and compute its backhaul capacity Z_i.
5: Compute SINR between each UE and ABS.
6: **for** each UE j **do**
7:     Sort the list of possibly serving ABS M_j according to their experienced $SINR$, in descending order.
8:     **for** $k = 1$ to $M_j.size$ **do**
9:         $cand \leftarrow M_j[k]$; Compute the required rate $R_{j,cand}$
10:         **if** $R_{j,cand} \leq Z_{cand}$ **then**
11:             $L_{cand} \leftarrow L_{cand} + j$;
            $Z_{cand} \leftarrow Z_{cand} - SINR_{j,cand}$
12:         break;
13: **return** L

Where N is the size of the population, $rand$ is a uniform random distribution over $[0, 1]$ and $floor$ is the integer part of the real number. As a result, the number of male members N_f is calculated as: $N_m = pop_{size} - N_f$.

A weight w_i is assigned to each spider i, to indicate the quality of its corresponding solution, and is computed as: $w_i = \frac{J(s_i) - worst_s}{best_s - worst_s}$ where $J(s_i)$ refers to the fitness value of the solution represented by the spider i and reflecting the objective function defined in (7). $best_s$ and $worst_s$ represent the best and the worst fitness value of the population, respectively.

Evaluating the quality of a spider's solution is carried out by the joint association of UEs with their serving ABSs and the ABSs association with the GBSs providing the backhaul link. Here, we propose a heuristic algorithm inspired by [51], that assigns each UE to its serving ABS. First, each ABS i is associated to the GBS providing the highest SINR, to maximize its backhaul capacity Z_i. Each UE j is then associated to the ABS providing the highest SINR if it has a sufficient backhaul capacity as shown in Algorithm 2

2) Information Exchange: The coordination between the members of the population is enabled by the exchanged messages between individuals. These messages are encoded as small vibrations and transmitted over the communal web. The vibrations perceived by the spider i from the spider j are expressed as follows: $Vib_{i,j} = w_j \cdot e^{-d_{i,j}^2}$ where $d_{i,j}$ is the Euclidean distance between the individuals i and j. Mainly, three special communications between spiders are considered:

- $Vibc_i$: information received by individual i, from individual s_c. s_c being the closest spider to i that holds a better weight, i.e. $w_c > w_i$,
- $Vibb_i$: information received by individual i, from individual s_b. s_b being the spider that possesses the better weight in the colony, i.e. $w_b = \max_{k \in \{1,2...pop_{size}\}} w_k$,
- $Vibf_i$: information received by spider i, from spider s_f: $Vibf_i$. s_f being the closest female spider to i.

3) Moving Spiders: In order to efficiently explore the search space, social spiders move and change their positions according

to their gender. We recognize two different operators: (i) A female operator and (ii) A male operator.

a) Female Operator: According to other members' vibrations, each female member demonstrates an attraction or repulsion behavior over them. This behavior is modeled as the position change of the female member i and depends on a combination of three different factors: the local best member s_c, the global best member s_b and a random factor.

The choice of attraction or repulsion is performed as a stochastic decision. Thus, the female's changing position is implemented according to the following formulas:

$$f_i^{k+1} = \begin{cases} f_i^k + \alpha \cdot Vibc_i \cdot (s_c - f_i^k) + \beta \cdot Vibb_i \cdot (s_b - f_i^k) \\ +\gamma \cdot (rand - 1/2) \text{ with probability } p_f \\ f_i^k - \alpha \cdot Vibc_i \cdot (s_c - f_i^k) - \beta \cdot Vibb_i \cdot (s_b - f_i^k) \\ -\gamma \cdot (rand - 1/2) \text{ with probability } 1 - p_f \end{cases}$$

b) Male Operator: According to their weight, male spiders are classified into two groups:

- Dominant males: they show an attraction behavior to the closest female individual s_f to perform mating.
- Non-dominant males: they are attracted to the weighted mean of the male individuals, so as to benefit from their underemployed resources.

Thus, the male's changing position is implemented according to the following formulas:

$$m_i^{k+1} = \begin{cases} m_i^k + \alpha \cdot Vibf_i \cdot (s_f - m_i^k) + \gamma \cdot (rand - 1/2) \\ \quad \text{for dominant males} \\ m_i^k + \alpha \cdot \left(\frac{\sum_{h=1}^{N_m} m_h^k \cdot w_{N_f+h}}{\sum_{h=1}^{N_m} w_{N_f+h}} \right) \text{ for non-dominant males} \end{cases}$$
(9)

4) Mating Operator: The mating operation is carried out by a dominant male member m_m, with a set E^f of the closest female individuals, located within its influence radius r, in order to produce a new off-spring solution. The resulting brood's solution is a combination of its parents $E^{mat} = E^f \cap m_m$ configurations. The weights of each parent determine their effect on the new brood solution. This is achieved by the weight proportionate selection mechanism, also known as the roulette wheel method. More precisely the probability p_i designing the influence of the parent $i \in E^{mat}$ is calculated as: $p_i = \frac{w_i}{\sum_{j \in E^{mat}} w_j}$.

The proposed SSO algorithm and the aforementioned steps are summarized in Algorithm 3.

V. MACHINE LEARNING FOR MOBILITY PREDICTION

As explained in Section IV, our adaptive SSO-based framework collects the predicted location of users once every time slot τ. These locations are used to adapt the ABSs positioning strategy (as can be seen in Fig. 2), which will naturally impact the coverage rate of the system. Over the different mobility prediction models, using machine learning in 5 G networks is drawing tremendous interest, as it is able to process heterogeneous correlated data, and handle a high dimensional action space.Hence, we decided to adopt machine learning models, to predict the user's location.

Algorithm 3: SSO Algorithm.

```
1:   Input: pop_size, iter_max
2:   Output: S_best Best spider with best solution
3:   generate the initial population of spiders.
4:   Evaluate the fitness of each spider S_i
5:   iter ← 0
6:   while iter <= iter_max do
7:     iter ← iter + +
8:     Compute the weight of each spider S_i.
9:     Update each female/male position.
10:    for each spider S_i do
11:      evaluate fitness J(s_i)
12:      if J(s_i) > J_max then
13:      J_max ← J(s_i); S_best = S_i; iter ← 0
14:    Perform Mating.
15:    Evaluate the new off-spring S_0
16:    if J(s_0) > J_min then
17:      Replace the worst spider by the new offspring
18:   return S_best
```
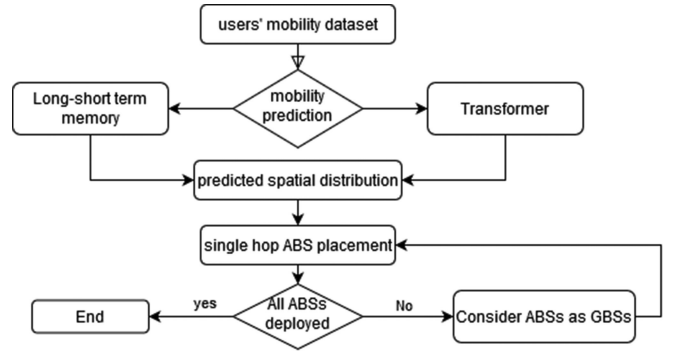

Fig. 2.   Adaptive SSO-based framework for ABSs placement.

Motivated by its remarkably increasing interest and improving performance in natural language processing, we decided to opt for the Transformer Model to predict the user's location. As a reference, we use the well-known special Recurrent Neural Networks (RNN) model called the e long short-term memory (LSTM), as it is famous for its suitability to handle sequence dependencies. We present these supervised machine learning approaches in the following.

A. Long-Short Term Memory (LSTM) Encoder-Decoder Architecture

Here, we present an LSTM-based encoder-decoder scheme for multivariate times series. We first introduce the LSTM unit and then explain the Encoder-Decoder architecture.

1) The LSTM Unit: The long short-term memory (LSTM) is a powerful kind of RNNs that was created to overcome the vanishing gradient issue in naively designed RNNs [52]. In LSTM, the output results depend on both the current input and the previous ones. The LSTM consists of an input layer, an output layer, and at least a hidden layer. It uses a combination of a memory cell c and a gating mechanism that controls the

information flow between the input, output, and memory cell. Three types of gates are distinguished:

- forget gate f: determines how much information from previous state should be retained,
- input gate i: determines if the input has to be remembered,
- output gate o: determines which information the cell memory should output.

2) Encoder-Decoder: The LSTM encoder-decoder model was first introduced for machine translation tasks [53] as it is able to learn and map sequences of different length. The model consists of two LSTM networks: the encoder and the decoder. The input sequence is processed by the LSTM encoder, that learns a fixed-length vector representation of it. This representation is passed to the LSTM decoder, that used it in the reconstruction of the target sequence using the previously predicted value and the current hidden state.

Given Y, $h^{(i)}$ is the hidden state of the encoder at time t_i for each $i \in \{1, 2, \ldots, T\}$, and $h'^{(j)}$ is the hidden state of the decoder at time t_j for each $j \in \{1, 2, \ldots, T'\}$ where $h^{(i)} \in R^c$, $h'^j \in R^{c'}$, c and c' represent the number of LSTM units in the hidden layer of the encoder and the decoder, respectively.

As introduced in [54], the LSTM encoder-decoder is trained to predict the coordinates sequence in reverse order; which means that the output time-series is $\{y^{(T)}, y^{(T-1)}, \ldots, y^{(1)}\}$. At instant t_i, the value $y^{(i)}$ and the hidden state $h^{(i-1)}$ of the encoder at instant $t_{(i-1)}$ are used by the encoder, in order to compute the hidden state $h^{(i)}$ of the encoder at instant t_i. The final hidden state of the encoder $h^{(T)}$ is used as the initial state for the decoder. A linear layer on top of the LSTM decoder network is used to predict the target: $y'^{(i)} = W.h'^{(i)} + b$, where W is a weight matrix and b is a bias vector.

During training, the decoder uses $y^{(i)}$ as input to obtain the state $h^{(i-1)}$, and then predicts $y'^{(i-1)}$ corresponding to target $y^{(i-1)}$. During inference, the predicted value $y'^{(i-1)}$ is input to the decoder to obtain $h'^{(i-1)}$ and predict $y'^{(i-1)}$. The prediction error $e^{(i)}$ for a point $y^{(i)}$ is given by: $e^{(i)} = \|y^{(i)} - y'^{(i)}\|$. Model training aims to minimize the objective $\sum_{Y \in s_N} \sum_{i=1}^{T} e^{(i)}$ where s_N is a set of training sequences.

B. The Transformer

The Transformer model was originally proposed by a Google team to solve machine translation problems [55]. It follows the encoder-decoder architecture, where the encoder maps the input sequence Y to a continuous sequence H. This latter is used by the decoder to generate the target sequence Y'. The model relies solely on attention mechanisms, dispensing with recurrence and convolutions. A positional-encoding is added to both input and output embedding in order to provide the model with the order of input and output sequences. The encoder consists of a stack of N_x identical layers. Each layer contains a multi-head self-attention and point-wise, feed-forward network (FFN) layer. The multi-head layer allows the use of multiple attention functions, while the FFN layer consists of a fully connected network used to process the attention layer. A residual connection followed by a normalization layer [56] is applied around both multi-head
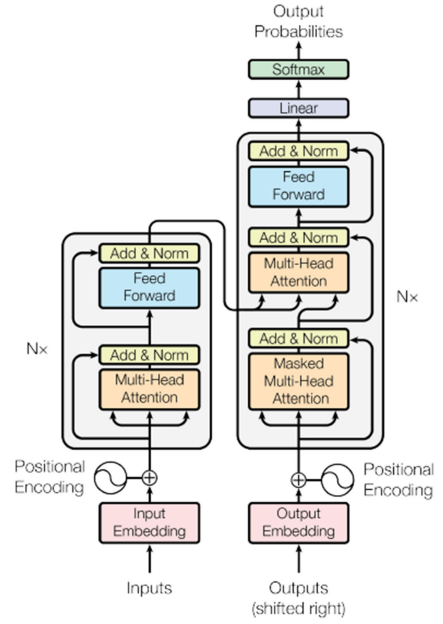

Fig. 3. Transformer model architecture [55].

and feed-forward network layers as shown in the left half of Fig. 3. The decoder architecture is similar to the encoder one. In addition to the stacked multi-head attention and the FFN layer, the encoder uses an additional multi-head attention layer to perform over the output of the encoder stack as shown in the right half of Fig. 3.

Thanks to the multi-head self-attention mechanism, the Transformer can focus simultaneously on different parts of the input. In the next section we present the self attention mechanism. The design and functioning of the multi-head attention is detailed thereafter.

1) Self Attention in the Transformer: Given the input time-series Y as defined above, each user's coordinates point $Y^{(i)}$ is such as $Y^{(i)} \in R^2$, i.e. $Y \in R^{T \times 2}$. The self-attention model starts by assigning a query q^i, a key k^i and a value v^i to each $Y^{(i)}$. The set of queries $Q \in R^{T \times 2}$, keys $K \in R^{T \times 2}$ and values $V \in R^{T \times 2}$ are computed using three different linear projection matrices W^Q, W^K and W^V, respectively. Where: $Q = Y \times W^Q$, $K = Y \times W^k$, and $V = Y \times W^V$.

The particular Scaled Dot-Product is then applied to the queries, keys, and values. This is achieved by computing the dot products of each query with all keys, dividing each by $\sqrt{d_q}$ where d_q is the query's dimension, and applying a softmax function to obtain the weights on the values. The matrix of outputs is conducted as: $Attention(Q, K, V) = Softmax(\frac{QK^T}{\sqrt{d_q}})V$

This attention is often called self-attention, as it builds a representation of the input sentence that is attentive to itself.

2) Multi-Head Attention: For a multi-head attention model with h heads, the query, key, and value are linearly projected h times with different linear learned projections. This allows the model to jointly attend to information from different representations. The attention function is then performed on each of the h projected queries, keys, and values. Finally, the attention's

TABLE II
TABLE OF NOTATIONS

Notation	Description
K	Set of GBSs
N	Set of UEs
M	Set of ABSs
V_{max}	UAV's maximum moving speed
V_i	Coordinates of GBSs
$U_i^{(t)}$	Coordinates of ABS i at time slot t
$Y_i^{(t)}$	Coordinates of user i at time slot t
$Y_i'^{(t)}$	Predicted coordinates of user i at time slot t
$P_k^{(t)}$	Transmission power of BS k at instant t
$I_{nm}^{(t)}$	User n being served by ABS m at instant t
$j_{lk}^{(t)}$	ABS l getting backhaul from BS k at instant t
$S^{(t)}$	Total number of served UEs at instant t
$Z_m^{(t)}$	Required backhaul capacity for ABS m

TABLE III
BASIC PARAMETERS

Parameter	Value
Environment	Sub-urban
Carrier frequency	2GHz
ABSs/GBSs bandwidth	20/20 MHz
V_{max}	50 m/s
Tx power of ABS	36dBm
Tx power of GBS	41dBm
SINR threshold	-7dB
GBS hight	25m
UEs hight	1.5m

TABLE IV
SCENARIOS' SPECIFICATIONS

Scenario	Simulation area	GBSs	UEs	ABS
small	2000m ×2000m	1	100	10
medium	4000m ×4000m	2	200	10
large	5000m ×5000m	3	400	15

TABLE V
CONTROL-PARAMETERS USED TO TRAIN RECURRENT AND TRANSFORMER MODELS

encoder-decoder type	LSTM	Transformer
hidden units	1024	512
encoder depth	4	6
decoder depth	4	6
batch size	128	2048

TABLE VI
MULTI-HOP SCENARIOS SPECIFICATIONS

Scenario	UEs number	ABSs number
1	100	3, 5, 8, 10, 13, 15
2	200	4, 8, 12, 16, 20
3	400	5, 10, 15, 20, 25

output of the h heads are then concatenated and the resulting vector is fed to a linear feed-forward network:

$MultiHead(Q,K,V) = Concat(head_1, head_2, \ldots, head_h)W^o$

$head_i = Attention(QW_i^Q, KW_i^K, VW_i^V)$

Where W_i^Q, W_i^K, W_i^V, and W^o are the linear projection matrices.

VI. PERFORMANCES EVALUATION

In the following, we present the computational experiments that were carried out to evaluate the performances of our multi-hop adaptive SSO-based framework for the ABS's placement. Experiments are organized into four groups. First, we test and evaluate the mobility prediction models. The objective of the second part is to tune the SSO's parameters to their best values. After that, the third part of the simulations is dedicated to evaluating the performance of the adaptive framework that allows multi-hop backhaul links presenting a clear advantage over the simple single-hop link. Finally, we use our ASF along with mobility prediction models to arrange the ABS's deployment and adapt their positions according to the users' distribution. We compare the results with a traditional static GBS deployment. We first describe the environment where the simulations are conducted, then we present the results of the experiments.

A. Simulation Scenarios

In order to simulate a realistic scenario where the deployment of ABSs is meaningful, we consider a sub-urban area that contains several ground base stations in predefined locations. A set of UEs is uniformly scattered around GBs and can freely move within the considered area. A limited number of ABSs are made available to provide wireless communication to UE. The basic transmission parameters are summarized in Table III. Three different scenarios with different area sizes, UE, ABSs, and GBSs numbers are generated as illustrated in Table IV.

B. Part 1: Mobility Prediction Models

In this section, we test and evaluate the proposed learning algorithm for users' mobility prediction. We present the real-life used DataSet, the analysis approach and the training setting. After that, we provide a comparative analysis of the mobility prediction models.

1) DataSet Description: In this work, a widely used mobility DataSet, namely Geolife [57] is used. GeoLife is a DataSet of GPS traces that were collected by Microsoft Research Asia. It contains spatial and temporal information of 182 Users (mainly located in Beijing) recorded over a period of five years, from April 2007 to August 2012. We consider the first scenario in Table VI, which consists of a $2000m \times 2000m$ sub-urban area that contains a single GBS in a predefined location, and a set of 100 uncovered UEs uniformly scattered around its coverage area.

2) Analysis Approach: As explained in section III, the locations of each user are collected once every time slot τ. We consider that $\tau = 15min$ in what follows. This means that each day in the DataSet is a set of 96 samples. To meet the description of the depicted scenario, only the first 100 users are considered. We then translated and rescaled the longitude and latitude of users to stay within the $2000m \times 2000m$ sub-urban area. After that, the data was reprocessed and normalized using
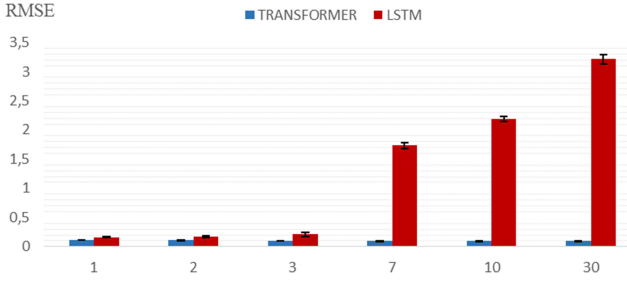
Fig. 4. Prediction accuracy of the users' location as a function of the size of input series.

the min-max method. Following the normalization step, the DataSet was variously divided into training, validation, and test sets but the best results were achieved with the repartition of a train set of 70 %, a validation set of 10 %, and a test set of 20 %. Afterward, the previously presented learning models are trained using the training data and the control parameters are optimized using the validation samples. We then, test the trained and validated learning models by applying them to the testing data. We evaluate the performance of the models using the Root Mean Square Error (RMSE) of the N predicted coordinates $(x,' y')$ to the real test data (x, y), which can be calculated as: $RMSE = \sqrt{\frac{1}{N} \sum_N (x' - x)^2 + (y' - y)^2}$.

3) Training Settings: The LSTM-based encoder-decoder is trained using the open-source Keras library [58], whereas the Transformer model experiments were carried out using the Tensor2Tensor toolkit [59]. Hence, the optimal training and inference parameters were selected in a preliminary stage for both approaches. To prevent over-fitting, we set the dropout [60] to 0.2 in the LSTM model and to 0.1 in the Transformer. Similarly, Adam optimizer [61] is used with an initial learning rate of 0.001 and 0.1 for LSTM and Transformer models, respectively. Table V summarizes the list of hyper-parameters.

4) Results: We first compare Transformer based and LSTM based models while varying the size of the input sequence. More precisely, the models process the input sequence that contains the users' locations in x days and predict their locations on the next day: $x \in \{1, 2, 3, 7, 10, 30\}$. Note that for each user, a day is a set of 96 timestamped locations. For each scenario, the results are presented in terms of average RMSE over the whole DataSet, with a 95% confidence interval (CI) and plotted in Fig. 4.

As shown in Fig. 4, the LSTM performance drastically decreases, as the input sequence length increases and the model becomes unable to accurately predict the users' locations. As opposed to the Transformer model that manages to maintain a generally stable behavior independently of the sequence length. This can be explained on the one hand, by the architectural limitation of the LSTM based model, that encodes the input sequence to a fixed-length internal representation. This imposes limits on the length of input sequences that can be reasonably learned. Besides, the information in RNN in general and LSTM, in particular, have been retained thanks to the previously computed hidden states and is then encoded and passed to the next time steps. This means that representation of the input is

strongly effected by the encoding of the previous input which results in a quick loss of information after a few time steps. On the other hand, the Transformer excludes any possibility of information loss as it has direct access to all the inputs simultaneously. Moreover, the self-attention mechanism allows processing both future and past elements and pays attention to relevant information, yielding a very good performance for both short and long input sequences.

We further investigate the performance of the LSTM and Transformer models as a function of the output sequence length. We train the models to use the users' location over 24 hours and predict the "next 12 hours" and "24 hours" locations. Using the same metric (RMSE), we compare the performances of the LSTM and Transformer models for each hour by averaging each day's result. The evaluation results of the "Next 12 hours" and "24 hours" are listed in Fig. 5, respectively. We notice that the Transformer model outperforms the LSTM model in each subfigure. Moreover, the advantage over the LSTM is more apparent for a relatively long-term "24 hours" prediction than a short "Next 12 hours" one. This demonstrates that the LSTM has difficulties when predicting relatively long sequences. In contrast, the Transformer model demonstrates a good performance for different sequence lengths.

Overall, better performance has been given with the Transformer compared to the LSTM encoder-decoder. The Self-attention-based Transformer produced a significant difference in performance with long input and/or output sequences.

C. Part 2: SSO Parameters Tuning

As described in Section IV-B, the proposed SSO has two global parameters: the number of search agents pop_{size} and the stopping condition, defined as the number of iterations without improvement of the global best solution $iter_{max}$.

We proceed to find the right values for pop_{Size} and $iter_{max}$. To do this, we considered static UEs with fixed locations and ran the algorithm on the previously mentioned medium scenario, while varying the value of pop_{Size} between 5 and 20, and $iter_{max}$ between 5 and 25. The experiment was repeated 15 times, each time with a different random seed. We then computed the percentage deviation between the best achieved solution SSO and the best solution achieved overall the runs J_{max} as: $GAP = \left(\frac{J_{max} - SSO}{J_{max}}\right) \times 100$. The experimental results are summarized in Fig 6 that shows the average GAP over all the runs, while Fig. 7 depicts the average runtime.

For all population sizes in Fig. 6, the average deviation (GAP) is decreasing and the solution quality is improving with the increase of $iter_{max}$. As $iter_{max}$ increases, the SSO keeps exploring new search areas and candidate solutions that improve the best solution's quality. More precisely, the values $iter_{max} = 25$ and $iter_{max} = 20$ lead to the best results in terms of solution quality. It is also shown that increasing the size of the population significantly improves the quality of the produced solution. Moreover, the graphical results show that the SSO could not find good solutions using a small population size of 5 or 10 spiders. It needs at least 15 spiders for achieving better solutions. The further increase in the size of the population does not lead
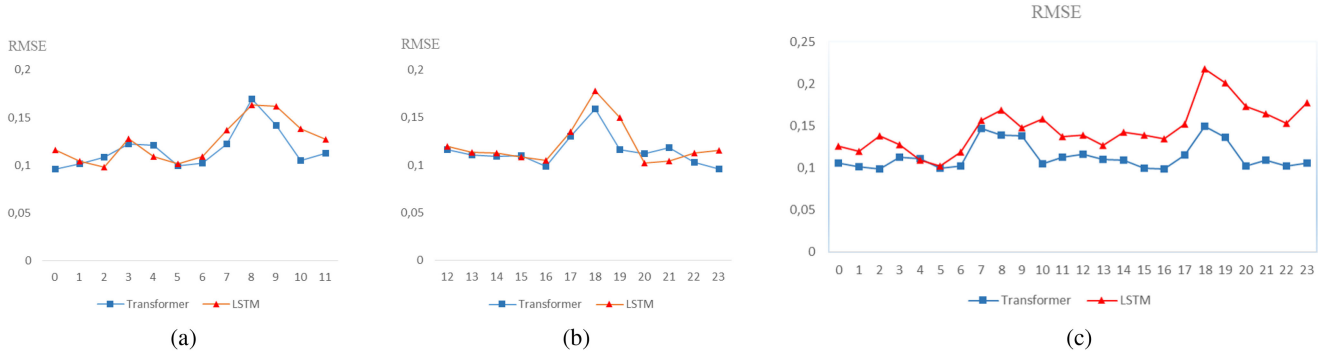
Fig. 5. Hourly average prediction accuracy of users' location in the next 12 hours and 24 hours. (a) First 12 hours of the day, (b) Last 12 hours of the day, (c) Next 24 hours.
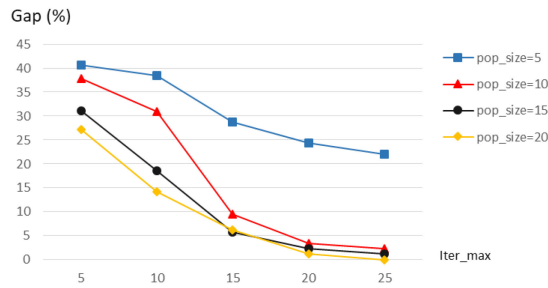

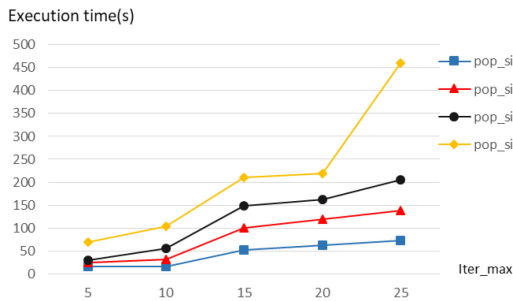Fig. 6. Effects of pop_{size} and $iter_{max}$ on solution quality.

Fig. 7. Effects of pop_{size} and $iter_{max}$ on the execution time.

to significantly better results (less than 2% for $iter_{max} \geq 20$). The subsequent increase in the population size leads only to an increase in computational time without significantly improving the GAP as can be seen in Fig. 7. The population size must be large enough for the solutions it contains to be diverse, but small enough for the algorithm to converge in a reasonable time.

Finally, the computational time of the metaheuristic is controlled by the parameters $iter_{max}$ and pop_{size}, and by changing their value, we achieve different trade-offs in terms of solution quality and computational effort. In order to maintain a good compromise between the quality of the solution and the execution time, we opted in the following to set $pop_{size} = 15$ and $iter_{max} = 20$.

D. Part 3: Adaptive SSO-Based Framework's Evaluation

In this section, we evaluate the performance of the multi-hop adaptive SSO-based framework. We review the improvement

that it could offer over the single-hop deployment solution. Then, we carry out a comparison between its results and those of two other multi-hop schemes:

- The multi-hop random search (MRS) algorithm: This scheme is based on the random search algorithm [62]. Indeed, it tries a specific number of randomly chosen positions of UAVs in the search space. The UAVs are jointly associated with the UEs and the backhauling BSs and the number of covered UEs is calculated. Finally, the positions with the highest coverage rate is retained as the optimum solution.
- The multi-hop uniform deployment (MUD): This method uniformly deploys the ABSs over the considered area. The UAVs are jointly associated with the UEs and the backhauling BSs and the number of covered UEs is calculated.

First, we consider the same $4000m \times 4000m$ area, where a single GBS is deployed, and try different users' densities. The number of UEs varies between {100, 200, and 400} for the scenarios {1, 2, and 3}, respectively. We consider a single time slot τ and use a different number of ABSs as illustrated in Table.VI. We check the behavior of both single-hop and multi-hop approaches and record their achievable coverage rates. The results of both single and multi-hop schemes were obtained with 15 runs of each algorithm with each number of ABSs on each scenario. Fig. 8 depicts the mean values of the ratio of served UEs using the multi-hop scheme compared with those obtained with the single-hop strategy.

From the first scenario's results, we can notice that the single-hop and multi-hop algorithms show the same coverage rates for small numbers of ABSs (3 and 5), as they both tend to place the ABSs around the GBS that provides a direct backhaul connection. A more remarkable coverage gain occurs with the increase of the number of ABSs for the multi-hop scheme as compared to the single-hop algorithm. The multi-hop scheme reaches a coverage rate of 96%, against 87% for the single-hop algorithm with the same 15 ABSs. This can be justified by the efficiency of the multi-hop algorithm in placing ABSs beyond the direct backhaul link. In other words, ABSs can be placed away from the GBS as they can get backhaul connections from other deployed ABSs. This allows them to reach more UEs and provide better coverage rates.
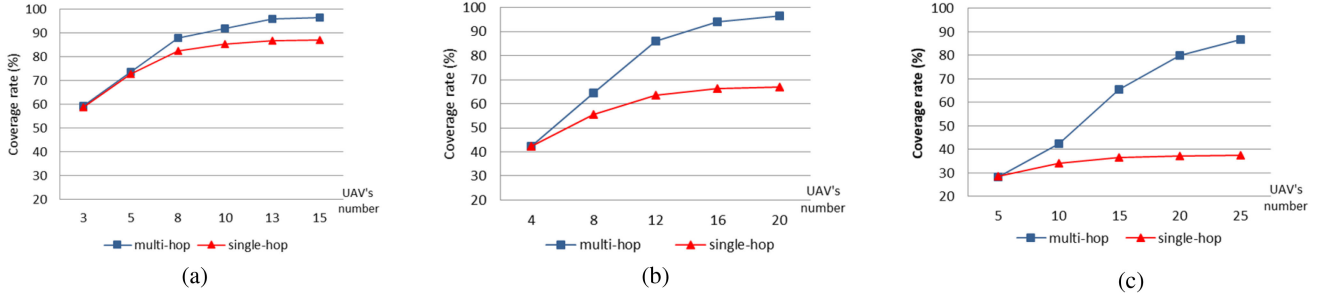
Fig. 8. Average number of served users with multi-hop and single-hop schemes. (a) scenario 1: 100 users, (b) scenario 2: 200 users, (c) scenario 3: 400 users.
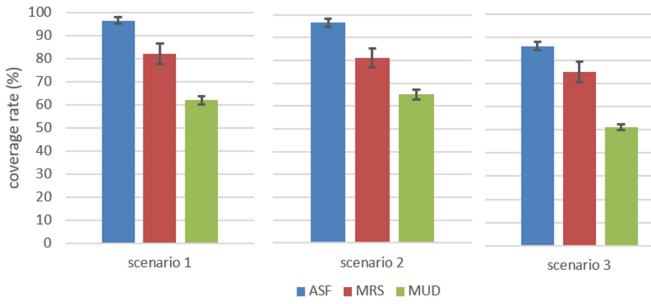

Fig. 9. Average coverage rate for ASF, MRS and MUD for the three scenarios.

Fig. 10. Average coverage rate calculated every 15 min during 4 hours.

Similar behaviors are noticed with the second and third scenarios, where the gap between the single-hop and multi-hop schemes is more remarkable. With the increase of user density, we can notice that on the one hand, the single-hop becomes unable to provide good coverage rates, as compared to the multi-hop algorithm. Indeed, direct backhaul toward the GBS is insufficient to provide service to all the users. Even when we deploy more ABSs, they are not used by the single hop algorithm as there is no backhaul link to establish. As a result, same poor coverage rates are obtained with 16 and 20 ABSs for the 2nd scenario and with 15, 20, and 25 ABSs for the 3rd. On the other hand, the multi-hop algorithm achieves better performance and offers maximum coverage rates of 96% and 86% while the single-hop only covers 67% and 37% of users in the 2nd and 3rd scenarios, respectively.

Fig. 9 depicts the mean values and the 95% CI of the coverage rates of our proposed multi-hop adaptive SSO-based framework (ASF), compared to those of the multi-hop random search (MRS) and the multi-hop uniform deployment (MUD) schemes, for the three aforementioned scenarios.

As can be seen, our ASF clearly outperforms both the MRS and the MUD schemes, for all the scenarios. On one hand, the MRS strategy tends to explore the search space by positioning the ABSs randomly, which provides a total average coverage of 79%. While, the MUD places the ABSs uniformly over the search space. Both schemes do not consider the UEs distribution, nor the GBSs positions, which leads to low coverage rates of 79% and 58% for the MRS and the MUD schemes, respectively. On the other hand, our ASF considers the UEs' and the GBSs' positions. Besides, our ASF uses different search agents
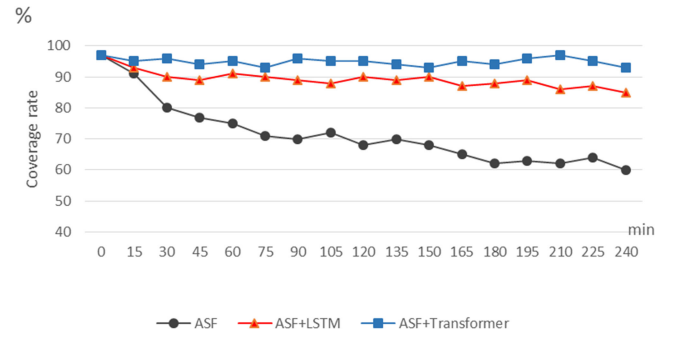
(spiders) to efficiently explore the candidate solution's domain by exchanging information about the best encounters solutions, leading to better performance and larger average coverage rates of almost 92%.

E. Part 4: Coverage Extension Based on Mobility Prediction

In this section, we investigate the effect of user mobility on the performance of our multi-hop placement algorithm and how can mobility prediction models help improve it and unveil the benefit of mobile ABSs, over traditional static GBS deployment. To this end, we consider four different schemes:

- GBSs deployment with unlimited backhaul capacity;
- Our adaptive SSO-based framework (ASF);
- ASF with the LSTM-based mobility prediction model;
- ASF with the Transformer-based prediction model.

The basic ASF considers fixed ABSs that do not change their positions during the mission. Whereas ASF with the LSTM and Transformer based predictions use the predicted locations of mobile users to anticipate their movement and plan the optimal ABSs placement for each time slot τ before the beginning of the coverage extension mission. We assess the coverage rate of the 4 schemes each $15min$ during $4 hours$. The results are depicted in Fig. 10.

As we compare the results of the above schemes, it can be seen that they all begin with a relatively high coverage rate of 96%. Despite the GBS's high backhaul capacity as compared to the ABS's limited one, similar behaviours are noticed, where the average coverage rate decreases over time and drops from 96% to 69% for the static GBS deployment and from 96% to 60% for ASF by the end of the 4 $hours$. As time passes, the UEs move,

change their positions and keep getting out of the GBS and static ABS coverage area yielding a loss of 36% and 45% of coverage rate for the GBS and static ASF deployments, respectively. Using the LSTM and Transformer based mobility prediction results allows the ASF to predict the spatial distribution of users over time and use the ABS's mobility to adapt the positioning according to the UE's mobility. Consequently, better coverage rates are notice and a loss of only 12% and 5% of coverage during the $4hours$ is recorded with the LSTM and Transformer models, respectively. It is also worth mentioning that, performance analysis shows that the transformer has given better coverage performances as compared to LSTM encoder-decoder. Indeed, the Transformer model outperforms the LSTM model in predicting users' mobility as shown in section VI-B

VII. CONCLUSION

In this paper, a general multi-hop ABS-assisted 5 G wireless network is considered, where unmanned aerial vehicles act as ABSs that dynamically extend GBSs' coverage without overloading the infrastructure. We propose a novel adaptive SSO-based Framework for 3D ABS placement, that exploits in conjunction with the SSO heuristic, predictive techniques to estimate accurately the spatio-temporal distribution of mobile users and adjust the ABSs position accordingly. Experimental results demonstrated the effectiveness of the multi-hop placement mechanism over the single-hop scheme for coverage extension especially with the increase of user density. Performance results clearly justify our use of machine learning model for users' mobility prediction. The prediction results further improve the placement efficiency and allow it to deliver better coverage rates. Given such performances, another study, which can be taken into consideration as future perspectives is the incorporation of reinforcement learning techniques in order to decentralize the control of ABS mobility and enable them to solely define their optimal coordinates.

REFERENCES

[1] C. V. N. Index, "Cisco annual internet report (2018–2023) white paper," White Paper, Mar. 2020.

[2] F. Lagum, I. Bor-Yaliniz, and H. Yanikomeroglu, "Strategic densification with UAV-BSs in cellular networks," *IEEE Wireless Commun. Lett.*, vol. 7, no. 3, pp. 384–387, Jun. 2018.

[3] A. A. Khuwaja, Y. Chen, N. Zhao, M.-S. Alouini, and P. Dobbins, "A survey of channel modeling for UAV communications," *IEEE Commun. Surv. Tut.*, vol. 20, no. 4, pp. 2804–2821, Oct.–Dec. 2018.

[4] N. Zhao *et al.*, "UAV-assisted emergency networks in disasters," *IEEE Wireless Commun.*, vol. 26, no. 1, pp. 45–51, Feb. 2019.

[5] M. Mozaffari, W. Saad, M. Bennis, Y.-H. Nam, and M. Debbah, "A tutorial on UAVs for wireless networks: Applications, challenges, and open problems," *IEEE Commun. Surv. Tut.*, vol. 21, no. 3, pp. 2334–2360, Jul.–Sep. 2019.

[6] A. Fotouhi *et al.*, "Survey on UAV cellular communications: Practical aspects, standardization advancements, regulation, and security challenges," *IEEE Commun. Surv. Tut.*, vol. 21, no. 4, pp. 3417–3442, Oct.–Dec. 2019.

[7] D. W. Matolak and R. Sun, "Air-ground channel characterization for unmanned aircraft systems–Part III: The suburban and near-urban environments," *IEEE Trans. Veh. Technol.*, vol. 66, no. 8, pp. 6607–6618, Aug. 2017.

[8] Y. Zeng, X. Xu, and R. Zhang, "Trajectory design for completion time minimization in UAV-enabled multicasting," *IEEE Trans. Wireless Commun.*, vol. 17, no. 4, pp. 2233–2246, Apr. 2018.

[9] H. Huang and A. V. Savkin, "An algorithm of efficient proactive placement of autonomous drones for maximum coverage in cellular networks," *IEEE Wireless Commun. Lett.*, vol. 7, no. 6, pp. 994–997, Dec. 2018.

[10] C. Caillouet, F. Giroire, and T. Razafindralambo, "Optimization of mobile sensor coverage with UAVs," in *Proc. IEEE Conf. Comput. Commun. Workshops*, 2018, pp. 622–627.

[11] M. Mozaffari, A. T. Z. Kasgari, W. Saad, M. Bennis, and M. Debbah, "3D cellular network architecture with drones for beyond 5G," in *Proc. IEEE Glob. Commun. Conf.*, 2018, pp. 1–6.

[12] M. Mozaffari, W. Saad, M. Bennis, and M. Debbah, "Drone small cells in the clouds: Design, deployment and performance analysis," in *Proc. IEEE Glob. Commun. Conf.*, 2015, pp. 1–6.

[13] E. Kalantari, M. Z. Shakir, H. Yanikomeroglu, and A. Yongacoglu, "Backhaul-aware robust 3D drone placement in 5G wireless networks," in *Proc. IEEE Int. Conf. Commun. Workshops*, 2017, pp. 109–114.

[14] R. I. Bor-Yaliniz, A. El-Keyi, and H. Yanikomeroglu, "Efficient 3-D placement of an aerial base station in next generation cellular networks," in *Proc. IEEE Int. Conf. Commun.*, 2016, pp. 1–5.

[15] M. Alzenad, A. El-Keyi, F. Lagum, and H. Yanikomeroglu, "3-D placement of an unmanned aerial vehicle base station (UAV-BS) for energy-efficient maximal coverage," *IEEE Wireless Commun. Lett.*, vol. 6, no. 4, pp. 434–437, Aug. 2017.

[16] E. Chaalal, L. Reynaud, and S. M. Senouci, "A social spider optimisation algorithm for 3D unmanned aerial base stations placement," in *Proc. IFIP Netw. Conf.*, 2020, pp. 544–548.

[17] M. C. Gonzalez, C. A. Hidalgo, and A.-L. Barabasi, "Understanding individual human mobility patterns," *Nature*, vol. 453, no. 7196, pp. 779–782, 2008.

[18] J. Chen and D. Gesbert, "Optimal positioning of flying relays for wireless networks: A los map approach," in *Proc. IEEE Int. Conf. Commun.*, 2017, pp. 1–6.

[19] Z. Becvar, M. Vondra, P. Mach, J. Plachy, and D. Gesbert, "Performance of mobile networks with UAVs: Can flying base stations substitute ultra-dense small cells?," in *Proc. 23th Eur. Wireless Conf.*, 2017, pp. 1–7.

[20] A. Al-Hourani, S. Kandeepan, and S. Lardner, "Optimal LAP altitude for maximum coverage," *IEEE Wireless Commun. Lett.*, vol. 3, no. 6, pp. 569–572, Dec. 2014.

[21] P. Zhan, K. Yu, and A. L. Swindlehurst, "Wireless relay communications using ANN unmanned aerial vehicle," in *Proc. IEEE 7th Workshop Signal Process. Adv. Wireless Commun.*, 2006, pp. 1–5.

[22] E. P. De Freitas *et al.*, "UAV relay network to support wsn connectivity," in *Proc. IEEE Int. Congr. Ultra Modern Telecommun. Control Syst.*, 2010, pp. 309–314.

[23] D. Orfanus, E. P. de Freitas, and F. Eliassen, "Self-organization as a supporting paradigm for military UAV relay networks," *IEEE Commun. Lett.*, vol. 20, no. 4, pp. 804–807, Apr. 2016.

[24] J. Korhonen, "Enhanced lte support for aerial vehicles," 3rd Generation Partnership Project (3GPP), Tech. Rep. 36.777, 2018.

[25] Y. Zheng, Y. Wang, and F. Meng, "Modeling and simulation of pathloss and fading for air-ground link of HAPs within a network simulator," in *Proc. IEEE Int. Conf. Cyber-Enabled Distrib. Comput. Knowl. Discov.*, 2013, pp. 421–426.

[26] J. Holis and P. Pechac, "Elevation dependent shadowing model for mobile communications via high altitude platforms in built-up areas," *IEEE Trans. Antennas Propag.*, vol. 56, no. 4, pp. 1078–1084, Apr. 2008.

[27] Q. Feng, E. K. Tameh, A. R. Nix, and J. McGeehan, "WLCp2-06: Modelling the likelihood of line-of-sight for air-to-ground radio propagation in urban environments," in *Proc. IEEE Globecom*, 2006, pp. 1–5.

[28] A. Al-Hourani, S. Kandeepan, and A. Jamalipour, "Modeling air-to-ground path loss for low altitude platforms in urban environments," in *Proc. IEEE Glob. Commun. Conf.*, 2014, pp. 2898–2904.

[29] W. Khawaja, I. Guvenc, D. W. Matolak, U.-C. Fiebig, and N. Schneckenburger, "A survey of air-to-ground propagation channel modeling for unmanned aerial vehicles," *IEEE Commun. Surv. Tut.*, vol. 21, no. 3, pp. 2361–2391, Jul.–Sep. 2019.

[30] Y. Zeng, R. Zhang, and T. J. Lim, "Wireless communications with unmanned aerial vehicles: Opportunities and challenges," *IEEE Commun. Mag.*, vol. 54, no. 5, pp. 36–42, May 2016.

[31] F. Jiang and A. L. Swindlehurst, "Optimization of UAV heading for the ground-to-air uplink," *IEEE J. Sel. Areas Commun.*, vol. 30, no. 5, pp. 993–1005, Jun. 2012.

[32] G. Zhang, Q. Wu, M. Cui, and R. Zhang, "Securing UAV communications via trajectory optimization," in *Proc. IEEE Glob. Commun. Conf.*, 2017, pp. 1–6.

[33] Y. Zeng, R. Zhang, and T. J. Lim, "Throughput maximization for UAV-enabled mobile relaying systems," *IEEE Trans. Commun.*, vol. 64, no. 12, pp. 4983–4996, Dec. 2016.

[34] J. Tisdale, Z. Kim, and J. K. Hedrick, "Autonomous UAV path planning and estimation," *IEEE Robot. Automat. Mag.*, vol. 16, no. 2, pp. 35–42, Jun. 2009.

[35] M.-A. Messous, H. Sedjelmaci, and S.-M. Senouci, "Implementing an emerging mobility model for a fleet of UAVs based on a fuzzy logic inference system," *Pervasive Mobile Comput.*, vol. 42, pp. 393–410, 2017.

[36] E. Kalantari, H. Yanikomeroglu, and A. Yongacoglu, "On the number and 3D placement of drone base stations in wireless cellular networks," in *Proc. IEEE 84th Veh. Technol. Conf.*, 2016, pp. 1–6.

[37] M. Mozaffari, W. Saad, M. Bennis, and M. Debbah, "Optimal transport theory for power-efficient deployment of unmanned aerial vehicles," in *Proc. IEEE Int. Conf. Commun.*, 2016, pp. 1–6.

[38] M. Mozaffari, W. Saad, M. Bennis, and M. Debbah, "Optimal transport theory for cell association in UAV-enabled cellular networks," *IEEE Commun. Lett.*, vol. 21, no. 9, pp. 2053–2056, Sep. 2017.

[39] I. Bor-Yaliniz and H. Yanikomeroglu, "The new frontier in RAN heterogeneity: Multi-tier drone-cells," *IEEE Commun. Mag.*, vol. 54, no. 11, pp. 48–55, Nov. 2016.

[40] B. Galkin, J. Kibilda, and L. A. DaSilva, "Backhaul for low-altitude UAVs in urban environments," in *Proc. IEEE Int. Conf. Commun.*, 2018, pp. 1–6.

[41] S. Chandrasekharan *et al.*, "Designing and implementing future aerial communication networks," *IEEE Commun. Mag.*, vol. 54, no. 5, pp. 26–34, May 2016.

[42] 3rd Generation Partnership Project; Technical Specification Group Radio Access Network, "Study on enhanced lte support for aerial vehicles," TR36.777 Release 15.

[43] 3rd Generation Partnership Project; Technical Specification Group Radio Access Network, "Study on channel model for frequencies from 0.5 to 100 ghz," TR36.873 Release 14.

[44] J. Li, Y. Zhou, L. Lamont, M. Toulgoat, and C. A. Rabbath, "Packet delay in UAV wireless networks under non-saturated traffic and channel fading conditions," *Wireless Pers. Commun.*, vol. 72, no. 2, pp. 1105–1123, 2013.

[45] C. E. Shannon, "Communication in the presence of noise," *Proc. IRE*, vol. 37, no. 1, pp. 10–21, 1949.

[46] C. Desset *et al.*, "Flexible power modeling of LTE base stations," in *Proc. IEEE Wireless Commun. Netw. Conf.*, 2012, pp. 2858–2862.

[47] C. D. Franco and G. Buttazzo, "Energy-aware coverage path planning of UAVs," in *Proc. IEEE Int. Conf. Auton. Robot Syst. Competitions*, 2015, pp. 111–117.

[48] Y. Zeng and R. Zhang, "Energy-efficient UAV communication with trajectory optimization," *IEEE Trans. Wireless Commun.*, vol. 16, no. 6, pp. 3747–3760, Jun. 2017.

[49] E. Cuevas, M. Cienfuegos, D. ZaldíVar, and M. Pérez-Cisneros, "A swarm optimization algorithm inspired in the behavior of the social-spider," *Expert Syst. Appl.*, vol. 40, no. 16, pp. 6374–6384, 2013.

[50] S. Z. Mirjalili, S. Saremi, and S. M. Mirjalili, "Designing evolutionary feedforward neural networks using social spider optimization algorithm," *Neural Comput. Appl.*, vol. 26, no. 8, pp. 1919–1928, 2015.

[51] J. Plachy, Z. Becvar, P. Mach, R. Marik, and M. Vondra, "Joint positioning of flying base stations and association of users: Evolutionary-based approach," *IEEE Access*, vol. 7, pp. 11454–11463, 2019.

[52] S. Hochreiter and J. Schmidhuber, "Long short-term memory," *Neural Computation*, vol. 9, no. 8, pp. 1735–1780, 1997.

[53] K. Cho *et al.*, "Learning phrase representations using rnn encoder-decoder for statistical machine translation," 2014, *arXiv:1406.1078*.

[54] I. Sutskever, O. Vinyals, and Q. V. Le, "Sequence to sequence learning with neural networks," in *Proc. Adv. Neural Inf. Process. Syst.*, 2014, pp. 3104–3112.

[55] A. Vaswani *et al.*, "Attention is all you need," *Adv. Neural Inf. Process. Syst.*, vol. 30, pp. 5998–6008, 2017.

[56] J. L. Ba, J. R. Kiros, and G. E. Hinton, "Layer normalization," 2016, *arXiv:1607.06450*.

[57] Y. Liu and H. S. Seah, "Points of interest recommendation from GPS trajectories," *Int. J. Geographical Inf. Sci.*, vol. 29, no. 6, pp. 953–979, 2015.

[58] C. François *et al.*, "Keras," 2015. [Online]. Available: https://github.com/fchollet/keras

[59] A. Vaswani *et al.*, "Tensor2tensor for neural machine translation," 2018, *arXiv:1803.07416*.

[60] N. Srivastava, G. Hinton, A. Krizhevsky, I. Sutskever, and R. Salakhutdinov, "Dropout: A simple way to prevent neural networks from overfitting," *J. Mach. Learn. Res.*, vol. 15, no. 1, pp. 1929–1958, 2014.

[61] D. P. Kingma and J. Ba, "Adam: A method for stochastic optimization," 2014, *arXiv:1412.6980*.

[62] J. Matyas, "Random optimization," *Automat. Remote Control*, vol. 26, no. 2, pp. 246–253, 1965.

Elhadja Chaalal (Student Member, IEEE) received the M.E. degree in computer science from Ecole Nationale Supérieure d'Informatique (National Higher School of Computer Science), Oued Smar, Algeria, in 2018. She is currently working toward the Ph.D. degree in computer science with Laboratory DRIVE EA 1859 Collocated, Institut supérieur de l'automobile et des transports, Nevers, France, and a part of the University of Burgundy, Dijon, France. She is conducting her Ph.D. research with Orange Labs, Chatillon, France. Her research interests include unmanned aerial vehicles, trajectory optimization, and network planning.

Sidi-Mohammed Senouci (Member, IEEE) received the Ph.D. degree in computer science from Sorbonne University, Paris, France, in October 2003, and the HDR degree from the Institut National Polytechnique de Toulouse, Toulouse, France. From December 2004 to August 2010, he was a Researcher with Orange Labs. Since September 2010, he has been a Professor with Institut supérieur de l'automobile et des transports (ISAT), Nevers, France, and a part of the University of Bourgogne, Dijon, France. Since October 2017, he has been also the Director with Laboratory DRIVE EA 1859 Collocated, ISAT. He has participated in several national and European-wide research projects such as, FP7 FOTsis, ITEA CarCoDe, ITEA PARFAIT, and ANR 5G-INSIGHT. He holds seven international patents and authored or coauthored his work in major IEEE conferences and renowned journals. He was the Co-Chair of VehiCom2009, IEEE Globecom2010, IEEE WCMC2010, IEEE Globecom 2011, IEEE ICC'2012, and IEEE ICC'2017. He was the Chair of IEEE ComSoc IIN Technical Committee, TCIIN during 2014–2016. He is a part of the Editorial Board of *IEEE Network Magazine* and a Guest Editor of premium journals, such as *ADHOC Journal*, *IEEE Network Magazine*, IEEE ACCESS, *IEEE Vehicular Technology Magazine*, and *French Journal REE*. He is also a Member of the Communications Society and Expert Senior of the French Society SEE (Society of Electricity and Electronics).
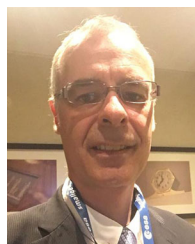
Laurent Reynaud (Senior Member, IEEE) received the Engineering degree from ESIGETEL, Villejuif, France, in 1996, and the Ph.D. degree in the domain of controlled mobility for drones and UAVs from the University of Lyon 1, Villeurbanne, France. He is currently a Senior Network Expert specialized into the performance of agile infrastructures for challenging environments. In 1997, he acquired a significant experience regarding the development and deployment of distributed software in the context of telecommunications, through successive positions with French Home Department, and with Alcatel-Lucent, Nokia, from 1998 to 2000. Since 2000, he has been with Orange, where he investigates the use of aerial and satellite connectivity to complement mobile networks terrestrial infrastructures. He participated in many French, European, and international cooperative research projects, including the domain of non-terrestrial networks via projects FP7 ABSOLUTE and ICT-19 5G!Drones. He has coauthored more than 50 conference and journal articles, and holds 12 international patents. His research interests include wireless multi-hop networks and the various issues related to non-terrestrial telecommunication platforms. He is the TPC Member or Reviewer for several ACM & IEEE conferences and journals.